# Wax Deposition in Stratified Oil/Water Flow

**ARTICLE** *in* ENERGY & FUELS · JUNE 2012

Impact Factor: 2.79 · DOI: 10.1021/ef2018989



Rainer Hoffmann
Linde Group



Sheng Zheng
University of Michigan



H. Scott Fogler
University of Michigan

energy&fuels

Article

pubs.acs.org/EF

# Wax Deposition in Stratified Oil/Water Flow

Rainer Hoffmann,*[,†] Lene Amundsen,[†] Zhenyu Huang,[‡] Sheng Zheng,[§] and H. Scott Fogler[§]

[†]Statoil ASA, Porsgrunn, N-3908, Norway

[‡]Multiphase Solutions Kenny Inc., Houston, Texas 77084, United States

[§]Department of Chemical Engineering, University of Michigan, Ann Arbor, Michigan 48103, United States

**ABSTRACT:** While diffusion as the major mechanism for wax deposition has been investigated in past decades, wax gelation has mostly been studied in quiescent conditions and is considered to be less significant than diffusion in flow conditions. In this study, gelation has been observed as a major mechanism for the formation of wax deposits in oil/water stratified flow. The experiments are carried out in a state-of-the-art flow loop using a North Sea gas condensate and formation water. The flow map study using reflex camera and X-ray tomography reveals that most of the completely stratified flows occur at low total flow rates of oil and water, which correspond to low shear stresses at the wall. It was found that the carbon number distributions of the wax deposits formed in this region have very low fractions of heavy components and are very close to the distribution of the deposit that is only formed by gelation. It was further revealed that the deposit thickness increases with increasing degree of gelation, which corresponds to decreasing shear stress of the fluids at the wall. This finding is consistent with previous studies from single-phase experiments where lower oil velocities are found to result in much higher deposit thicknesses and low wax fractions in the deposits.

## 1. INTRODUCTION

**1.A. Wax Deposition in Oil/Water Stratified Flow.** The understanding as well as the prediction of the rate of wax deposition from waxy oils in production pipes are crucial in field development and operations. Wax deposition can lead to a reduction in oil production, increased operational costs and Health, Safety, and Environment problems, and in some cases the pipeline can be plugged by having a pig stuck in the deposited gel. In all of the prevention and remediation methods in use (pigging, pipeline insulation, heating), the rate of wax deposition needs to be known a priori to choose and design the appropriate preventive or remediation techniques.

To predict wax deposition, new models are being used that take into account the properties of the gas condensate, the fluid flow, and the heat/mass transfer characteristics of the pipeline.[1,2,5] Of the various mechanisms that were discussed in the very first papers on pipeline wax deposition,[3] molecular diffusion is today considered to be the dominant mechanism. Because production pipelines field data are difficult to obtain (due to nonconstant conditions and insufficient instrumentation),[4] the common method to validate the basic assumptions of a deposition model is to perform experiments in a flow loop. To this end, a state-of-the-art 2 in. flow loop was constructed at the Statoil Research Centre Porsgrunn where real waxy gas condensate from a North Sea field flows through a test section where a surrounding water annulus simulates the conditions subsea.[16] This flow loop was used to study wax deposition for stratified oil/water flow, which is of great interest because most fields produce a significant amount of water, especially in their late life. This study investigates how an increasing water cut will influence wax deposition and the pigging frequency. (The term "water cut" describes the fraction of the water flow rate based on the total flow rate, $[Q_w/(Q_w + Q_o)]$, as an operating condition for the experiments.)

**1.B. Different Mechanisms for Deposit Formation.** Previous studies have shown that a wax deposit can be formed by two possible mechanisms: (1) diffusion of wax molecules from the bulk oil to the oil–deposit interface[5] and (2) gelation due to crystallization of wax molecules.[6−16] These two mechanisms will be further discussed in detail.

*Diffusion of Wax Molecules at the Oil/Deposit Interface.*[5] Because of the heat loss of the oil to the surroundings, the temperature of the wall decreases and wax molecules start to precipitate at the wall to form an incipient layer of deposit. This precipitation reduces the concentration of wax at the oil–deposit interface and generates a radial diffusion flux of wax molecules from the bulk toward the oil–deposit interface. The wax molecules that diffuse to the oil–deposit interface can either precipitate at the interface to increase the thickness of the existing deposit or continue to diffuse into the deposit and contribute to the increase of wax fraction in the deposit. This diffusion flux of the wax molecules (the heavy components) into the deposit is accompanied by the counter-diffusion flux of the oil molecules (the light components) from the deposit back to the oil phase. Consequently, the deposit resulting from these diffusion fluxes is enriched with heavy components. The trend was originally found by the study of Singh and Fogler as shown in Figure 1.[5]

*Gelation Due to the Crystallization of Wax Molecules.* The crystallization of wax in oil has been studied since the 1920s.[6] The crystal structures observed from optical microscopy for the *n*-paraffins formed under static conditions are mainly platelet-like crystals with diameters of 30−100 $\mu$m (Figure 2),[6−9] although the presence of the branched and cyclic

**Received:** December 3, 2011
**Revised:** May 24, 2012

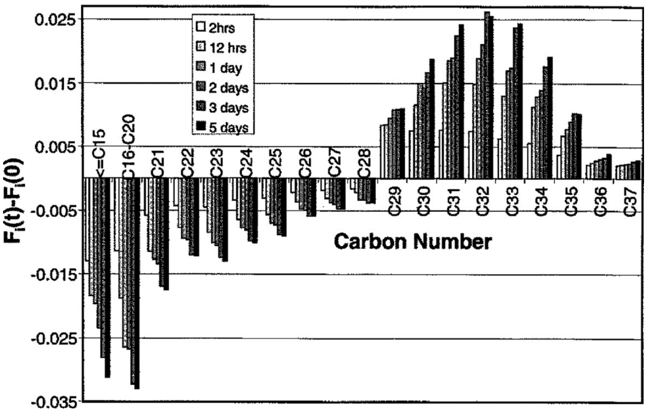


**Figure 1.** Change in carbon number distribution of gel deposits from flow loop with times.[5]

paraffins can significantly alter the structure and the crystallinity of the gel.[10,11]

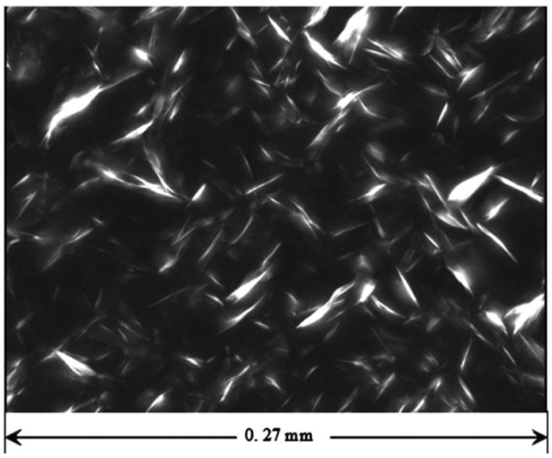


**Figure 2.** Wax crystals observed under cross-polarized microscopy by Venkatesan and Fogler.[9]

Kane et al. have used cryofixation with transmission electron microscopy (TEM) to reveal the microstructure of the wax crystals,[12] as shown in Figure 3.

It was found that the wax crystals consist of smaller "pine cone" blocks of around 3–5 $\mu$m. Each block includes the platelet structure with stratified lamellas of area around 0.5–1 $\mu m^2$. A closer examination at the surface of the lamella reveals that the platelet consist of disk-like subunits with diameters of 20–40 nm, which is considered to be the locations of the nucleation as the initial stage of wax crystallization. It is believed that the aggregation of these disk-like subunits forms the platelet lamellas, while the overlapping of the platelet lamellas forms the "pine cone" structures. It is believed that the aggregation of the "pine cone" structures forms the platelet crystals that one frequently sees in an optical microscope.[6−9]

As temperature further decreases from the cloud point, the degree of wax crystallization becomes sufficient to form a crystal network so that the entrapped oil is no longer able to flow. The mixture of the solid network and its entrained oil forms a gel. A number of studies on the structure of the network of wax crystals revealed that the growth of the wax crystals and the aggregation of the existing crystals occur simultaneously and that the network is connected by the attractive interactions between the wax crystals.[7]

Although wax gelation has been frequently observed in quiescent conditions, recent studies have focused on the investigation on the wax gel formed under shear/flow conditions.[9,12−14] Venkatesan et al. have shown that a model wax–oil system was still able to gel when the shear stress is as high as 5 Pa (corresponding to a flow rate of 16 000 barrels per day in a 10-in. pipeline with an oil viscosity of 10 cP at pipeline conditions).[9] The imposed shear rate is known to delay or suppress gelation, as reported by several rheological studies.[12−15] Kane et al. found that the shear stress can significantly reduce the gelation temperatures. This conclusion was found from the drastic increase of the apparent viscosity from their rheometer measurements as shown in Figure 4.

A summary of the conditions necessary for diffusion-formed deposit and gelation-formed deposition is listed in Table 1.

## 2. EXPERIMENTAL SETUP

**2.A. Wax Deposition Flow Loop Apparatus.** The state-of-the-art flow loop apparatus, also called a test rig, used for the experimental program is located in the Multiphase Flow Loop Laboratory at Statoil's Research Centre Porsgrunn, Norway. It is used to study wax deposition mechanisms and to develop technologies for wax removal, wax prevention, and wax thickness measurements. A schematic layout of the flow loop is shown in Figure 5.

Before an experiment begins, the water and oil phases are preheated separately using a oil heat exchanger. Preheated oil and water are continuously circulated in the flow loop using the water and oil pumps. The oil phase is circulated through the heat exchanger during the experiment to keep the oil temperature constant. Because there is no separate heat exchanger to keep the water temperature constant, the water temperature drops during the course of an experiment to a lower

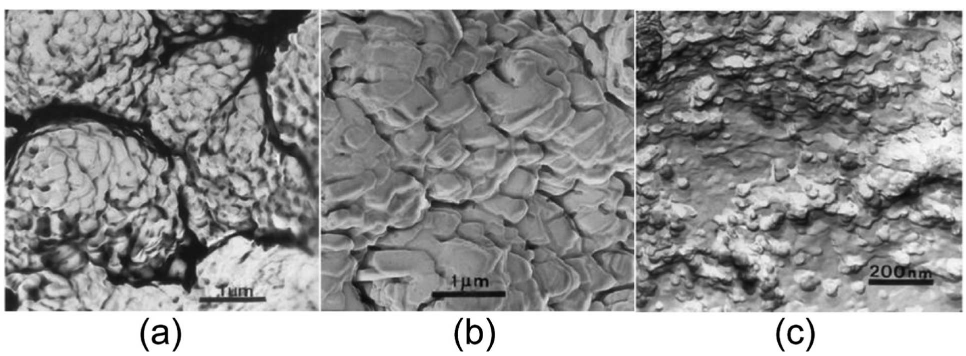


**Figure 3.** The microstructure of the wax crystals observed by Kane et al.[12] (a) The "pine cone" structure of paraffin crystallized from in the crude oil. (b) The wax platelet lamellas observed on each "pine cone" structures. (c) The disk-like subunits that form the platelet lamellas.


dx.doi.org/10.1021/ef2018989 | Energy Fuels XXXX, XXX, XXX−XXX

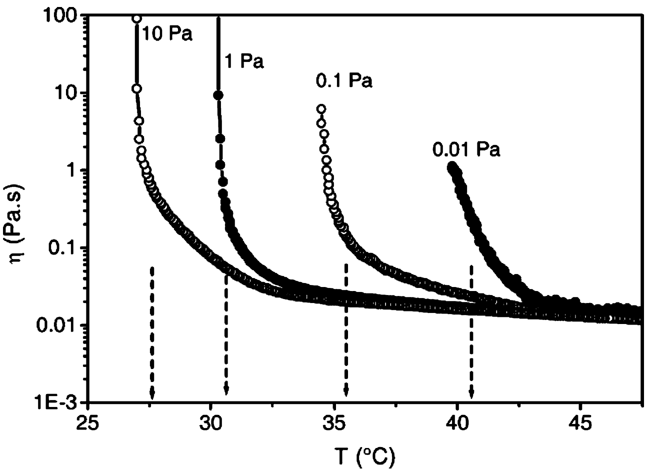


**Figure 4.** The impact of impose shear stress on gelation temperature from the study of Kane et al.[13] The gelation temperatures are highlighted with vertical dash lines where a steep increase of the apparent viscosity is observed. The cooling rate is 0.5 °C/min.

**Table 1. Summary of Conditions for Diffusion and Gelation as well as the Difference in the Amount of Heavy Components Formed by These Two Mechanisms**

| | diffusion | gelation-driven |
|---|---|---|
| prerequisites | radial temperature gradient, $T_{\mathrm{wall}}$ < WAT | $T \ll$ WAT, low shear rate |
| heavy component fraction in the deposit | higher than oil | low |

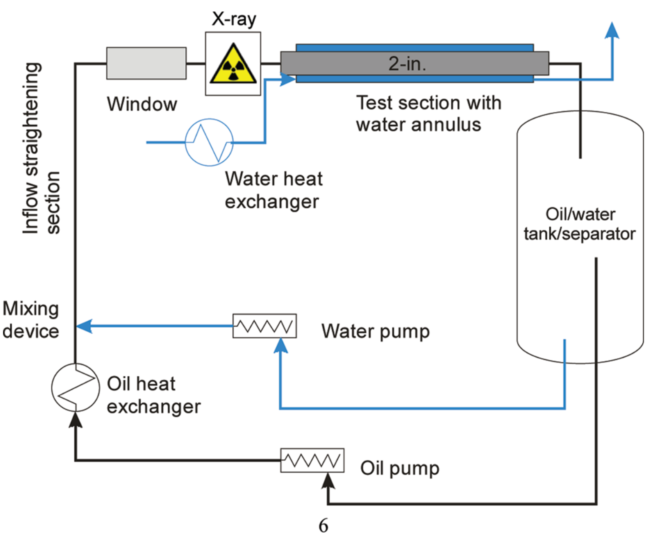


**Figure 5.** Wax deposition test rig − overview.

level, which is mainly defined by the ambient temperature. In a future modification, an additional heat exchanger for the water flow shall be implemented to avoid this drawback. The oil and water are unified in a Y-shaped mixing device, which initializes stratified flow by avoiding excessive mixing of the phases. Oil and water then flow through a 17 m long pipe section to ensure fully developed flow before entering the test section. After the inflow section, the flow enters first a window section for visual observations of the flow structure followed by an X-ray tomograph for measuring the phase distribution. Next, the fluids enter the 2-in. test section where they are cooled by water that is circulating in an annulus surrounding the oil pipe, simulating the conditions subsea. The coolant water is provided from the communal network and is heat exchanged with steam to achieve the specified temperature before entering the test section annulus.

After the test section, the two-phase flow returns to the tank where gravity separates them into clean phases that can be sent back into the rig. The large main separator with a maximum volume of 4.2 $m^3$ was designed to give a long retention time and to prevent wax depletion of the circulating oil. Density measurements in front of each pump are used to monitor the separation quality of the phases. Some key data for the rig may be found in Table 2.

**Table 2. Dimensions and the Operating Conditions for the Wax Deposition Rig**

| | |
|---|---|
| oil pipe − inner diameter | 52.5 mm |
| water annulus − inner diameter | 131.3 mm |
| whole test section length | 5.31 m |
| removable test section length | 0.63 m |
| tank − max volume | 4200 L |
| oil temperature | 10−60 °C |
| coolant water temperature | 5−60 °C |
| oil flow rate | 2−20 $m^3$/h |
| water flow rate | 2−20 $m^3$/h |
| coolant water flow rate | 3−16 $m^3$/h |
| pressure | 1 bar |

### 2.B. Laser-Based Measurement of Wax Deposit Distribution.

An important difference between multiphase wax deposition and single-phase wax deposition is that the resulting deposit is not necessarily uniformly distributed around the pipe circumference. Therefore, an additional measurement technique is required to document the wax thickness distribution.

To this end, the laser-based technique that was already used in the previous study[16] was extended. The basic idea is still the same: To project a laser light in a circle on the inner pipe wall, take a picture of this light circle and then calculate the pipe diameter from the diameter on the picture (see Figure 6). However, to quantify the circumferential distribution of wax, the method needed to be extended.

In the first step, a calibration curve is established that relates the diameter of the circle in the camera pictures (measured in pixels) to the real inner pipe diameter (in millimeter). To achieve the calibration curve, five pipes with diameters from 48 to 52 mm were manufactured. For each of these pipes, three laser measurements are performed.

Having determined the calibration curve, the measurement of the actual wax deposit can be performed. Figure 7 shows an example of an experiment with stratified oil/water flow where wax only deposited in the upper half of the pipe. The irregular shape of the deposit can be clearly determined in the shape of the laser light projection, which is no longer circular. To determine the center of the clean pipe, it is necessary to tell the algorithm which part to use for the circle fit. This instruction needs to be specified manually from the visual observations of the wax deposit. The points used in this case as representative points for the clean pipe are marked yellow in the upper right picture and black in the lower left picture. They are specified by first applying the algorithm for a clean pipe and then taking a subset of these points by defining a certain sector (see the lower left picture; in this case, the sector ranged from 30° to 160°, where 0° is east).

In the next step, the distance from the found pipe center to each of the points on the wax surface can be calculated first in pixels and then converted to millimeters using the calibration curve. Knowing the inner diameter for the empty pipe allows one to finally calculate the wax thickness as a function of the position around the circumference. This deposition is shown in Figure 7; it can be clearly seen that there is a plateau at the bottom of the pipe where the wax thickness is zero. The absolute thickness of the wax thickness from the laser measurements was double-checked by caliper measurements of the wax layer at the top of the pipe and by comparing the average thickness from the laser measurements with the weight measurements. Both comparisons showed agreements within 20%.


dx.doi.org/10.1021/ef2018989 | Energy Fuels XXXX, XXX, XXX−XXX


**Figure 6.** Laser-based measurement device.

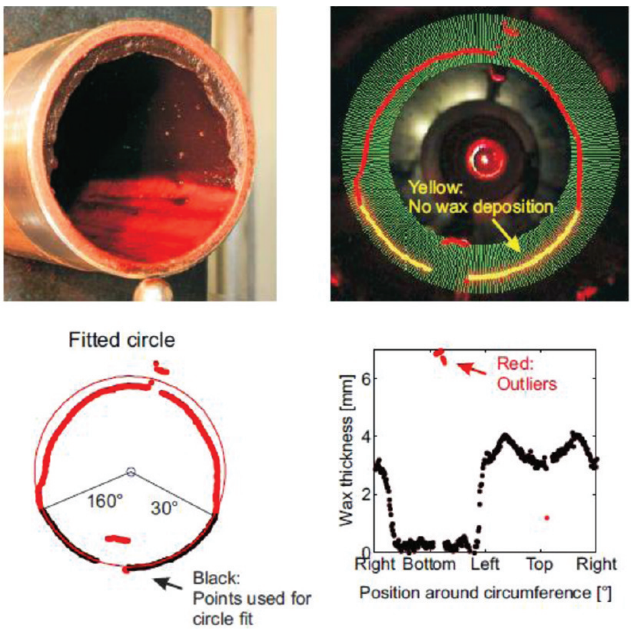


**Figure 7.** Laser measurement – wax deposit.

**2.C. X-ray Tomography.** An X-ray tomograph was used to measure the vertical phase distribution in the pipe before the flow enters the test section. The tomograph was built by Innospexion AS and consists of two pairs of X-ray sources and detectors, so that both the horizontal and the vertical phase distribution can be measured. The X-ray source is a water-cooled MB70 MCA 450 monoblock X-ray source with a maximum energy of 60 kVp. The detectors consist of CdTe CMOS detector arrays with 1500 pixel resolution.

The water volume fraction was calculated from X-ray measurements, which were performed over 30 s to average over all transient flow phenomena. The water volume fraction for a two-phase flow $\phi(x)$ as a function of the vertical position $x$ (see Figure 8) is calculated by comparing the measured X-ray intensities for oil–water flow $I_{ow}(x)$ with the intensities for single-phase oil flow $I_o(x)$ and single-phase water flow $I_w(x)$, which is shown in eq 1. A more in-depth description of the theory can be found in the research by Hoffmann and Johnson.[17]

$$\phi(x) = \frac{\ln \frac{I_{ow}(x)}{I_o(x)}}{\ln \frac{I_w(x)}{I_o(x)}} \quad (1)$$

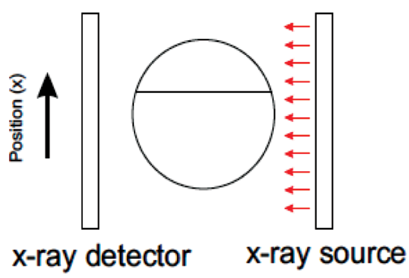


**Figure 8.** Layout of vertical X-ray measurement.

**2.D. Gas Chromotography.** Gas chromatography was used to measure the carbon number distributions of the deposit. The crude oil is measured using high temperature gas chromatograph (HTGC) Hewlett-Packard 6890A equipped with a CP-SimDist Ultimetal column (25 m × 0.53 mm × 0.09 mm). The oven temperature was initiated at 40 °C and increased to 430 °C at a rate of 10 °C/min.

**2.E. Fluid Characteristics.** *2.E.1. Oil and Water Composition.* The North Sea gas condensate utilized in this research is the same as that in the previously reported[16] single-phase study (4.7 wt % wax content, 30 °C WAT, $\eta$ = 3 cP @ 20 °C). The salt concentration of the water phase was chosen to be equal to the formation water from that field. The ion concentrations are listed in Table 3.

**Table 3. Water Composition**

| ion | concentration [mg/L] |
|---|---|
| sodium, Na | 158 |
| calcium, Ca | 16 |
| potassium, Ka | 204 |
| chloride, Cl | 735 |
| sulfate, $SO_4^{2-}$ | 33 |

*2.E.2. Surface Tension Oil/Water.* Pretests have shown that gravity separation in the tank is not sufficient to encourage oil/water phase separation to occur at lower temperatures and higher flow rates. It was therefore decided to add a commercially available emulsion breaker (DMO 86538, 500 ppm) to improve separation.

The interfacial tension of the system was measured at 20 °C by the pendant drop method, using Teclis equipment. Two measurements were performed, one where the sample was cooled quickly and one where the sample was cooled as slowly as possible. The estimated pseudoequilibrium interfacial tension was found to be ca. 11 mN/m, virtually independent of thermal history, which is a low value for a condensate sample. This low value is most likely due to the effect of the emulsion breaker.

It should be noted that comparison experiments have been carried out with oil, a negligible amount of water, and emulsion breaker in the tank. The amount of wax deposition is nearly the same as in previously single-phase experiments when there is only oil in the tank,[16] which indicates that the emulsion breaker would not significantly affect wax deposition.

## 3. RESULTS AND DISCUSSION

**3.A. Hydrodynamics.** The most interesting parameter in two-phase oil/water flow is of course the water cut. To

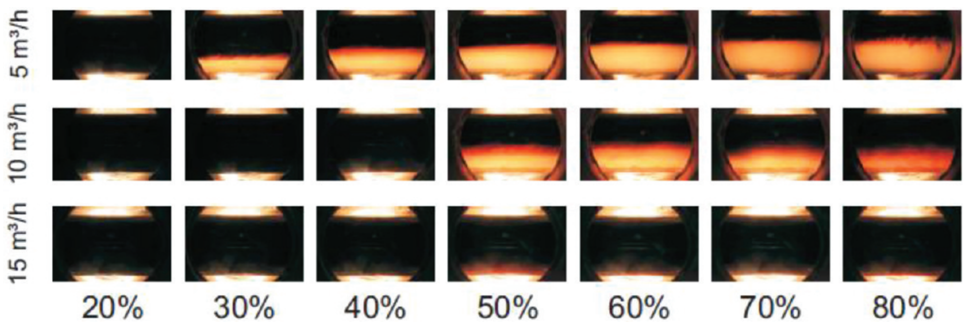


**Figure 9.** Camera picture at different water cuts.

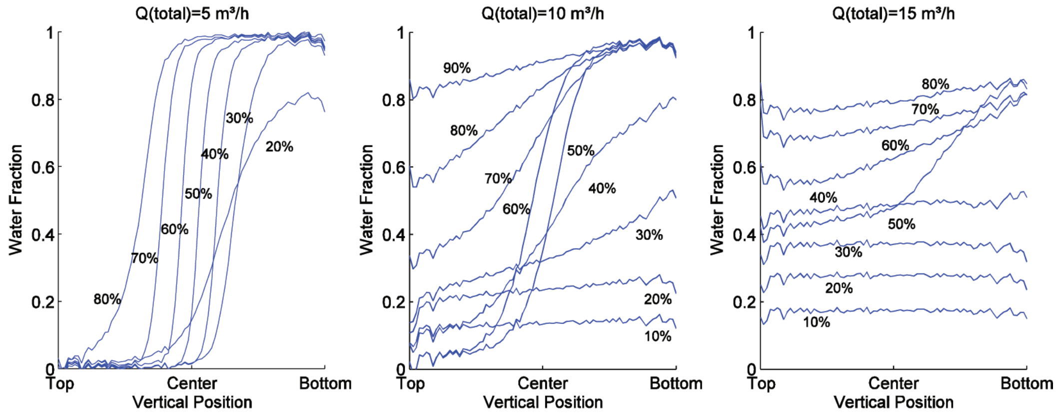


**Figure 10.** Water fraction at different water cuts — X-ray measurements.

investigate its influence and to define the matrix of most relevant wax deposition experiments, a prestudy was performed where the influence of the water cut on the flow regime was investigated.

Experiments were carried out for three different total volumetric flow rates. These two-phase flow rates were $Q_{total} = Q_o + Q_w = 5$ m$^3$/h, $Q_{total} = 10$ m$^3$/h, and $Q_{total} = 15$ m$^3$/h, corresponding to mixture velocities of $V_{total} = 0.64$ m/s, $V_{total} = 1.28$ m/s, and $V_{total} = 1.92$ m/s. Experiments were carried out with water cuts ranging from 10% to 80%. Figure 9 shows the photographic pictures for these flow regimes. It is observed that completely stratified flows occur for the case of water cut between 30% and 70% when the total flow rate is 5 m$^3$/h, while completely stratified flows occur in a smaller range of water cut (50−60%) as the total flow rate increases to 10 m$^3$/h. This observation confirmed the known fact that the degree of dispersion increases with increasing total flow rate.[18]

Visual impression, however, can be misleading because relatively small amounts of dispersed oil in water make the mixture appear dark. It was therefore important to measure the water volume fraction using the X-ray instrument. Figure 10 shows the water fraction distribution for the three flow rates.

Correspondingly to the reflex camera pictures, the lowest flow rate, 5 m$^3$/h, gave fine stratified flow regimes except at water cuts of 20% and 80%, where some dispersion was observed. For the flow rate of 10 m$^3$/h, there is a clear transition from fully dispersed flow at 10% and 20% water cut to stratified flow (around 40−70% water cut) and further on to water continuous flow. The highest flow rate of 15 m$^3$/h shows almost always fully dispersed flow with the exception of 50% water cut, which appears to be stratified flow of a water continuous and an oil continuous phase (albeit with a high amount of dispersion in each of the phases).

Because the scope of this study focuses on stratified flow, it was decided to perform one series of experiments with varying water cut at a total flow rate of 5 m$^3$/h and one series at a total flow rate of 10 m$^3$/h . In a later study, we plan to extend this investigation also to higher flow rates and dispersed flow.

**3.B. Deposit Characterization.** Two lists of deposition experiments are shown in Tables 4 and 5 for different total flow rates. It can be seen that the inlet temperatures for the oil and the coolant were not the same, which was due to the limited number of heat-exchanger available in the flow loop.

**Table 4. List of Operating Conditions for the Deposition Experiments with Different Water Cuts for the Total Flow Rate of 5 m$^3$/h**

| | | | | | | |
|---|---|---|---|---|---|---|
| total flow rate (m$^3$/h) | 5.0 | | | | | |
| water cut (%) | 0.0[a] | 25.0 | 50.0 | 65.0 | 75.0 | 80.0 |
| oil flow rate (m$^3$/h) | 5.0 | 3.7 | 2.5 | 1.7 | 1.2 | 1.0 |
| water flow rate (m$^3$/h) | 0.0 | 1.3 | 2.5 | 3.3 | 3.8 | 4.0 |
| duration (days) | 2.0 | 2.6 | 2.7 | 2.7 | 2.7 | 2.7 |
| oil inlet temperature | 24.0 | 24.0 | 24.0 | 24.7 | 25.0 | 24.4 |
| water inlet temperature | | 23.1 | 21.6 | 22.0 | 21.3 | 20.5 |
| coolant temperature (°C) | 15.0 | | | | | |

[a]The GC measurement is not available for these experiments.

*3.B.1. Investigation of Deposition Mechanism for the Wax Deposits by Gas Chromatography.* Not only do diffusion and gelation have different prerequisites, it is expected that these two types of mechanism should yield deposits with different compositions: Because a radial concentration gradient, a prerequisite for diffusion, is not required for gelation-formed deposition, there is no reason for an enrichment of heavy

**Table 5. List of Operating Conditions for the Deposition Experiments with Different Water Cuts for the Total Flow Rate of 10 $m^3/h$**

| | | | | | |
|---|---|---|---|---|---|
| total flow rate ($m^3/h$) | 10.0 | | | | |
| water cut (%) | 0.0[a] | 10.0 | 50.0 | 75.0 | 85.0 |
| oil flow rate ($m^3/h$) | 10.0 | 9.0 | 5.0 | 2.5 | 1.5 |
| water flow rate ($m^3/h$) | 0.0 | 1.0 | 5.0 | 7.5 | 8.5 |
| duration (days) | 1.8 | 2.8 | 1.8 | 1.7 | 1.8 |
| oil inlet temperature | 25.0 | 25.0 | 25.0 | 24.9 | 24.8 |
| water inlet temperature | | 24.6 | 23.5 | 22.9 | 22.5 |
| coolant temperature (°C) | 15.0 | | | | |

[a]The GC measurement is not available for these experiments.

components in a gelation-formed deposit. In other words, if one is to carry out a GC analysis of a deposit that is only formed by gelation, its carbon number distribution should be the same as that of the crude oil. As we have discussed previously that a diffusion-formed deposit consists of a higher fraction of heavy components than the crude oil, it must have a higher fraction of heavy components than a deposit that is gelation-formed, as is sketched in Figure 11.

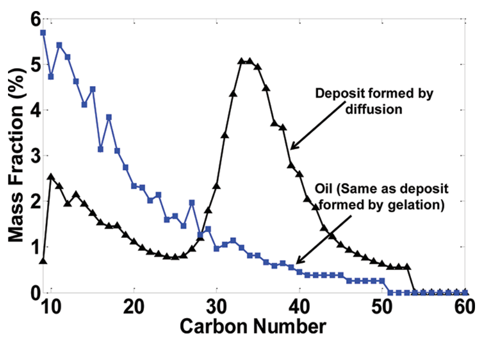


**Figure 11.** Comparison of the carbon number distributions from GC measurements between a diffusion-formed deposit and a gelation-formed deposit, which has the same carbon number distribution as the crude oil.

In the two-phase experiments in this study, the conditions for diffusion to occur are satisfied as the radial temperature gradient has been established by the heat loss from the oil and the water to the coolant and the wall temperature is less than WAT (30 °C). The shear stress at the wall is around 0.5−1 Pa for the oil phase, which is well within the reported range of the shear stress where gelation can occur (<5 Pa).[9] Therefore, both the gelation and the diffusion mechanisms can contribute to the formation of the wax deposit. It will be subsequently shown which mechanism is prevalent to the formation of the wax deposits at different water cuts.

Figure 12 shows the carbon number distribution from the GC measurements of the deposits for all of the experiments. A drastic difference can be seen between the carbon number distributions in the deposits for the experiments with different total flow rates. As compared to this difference, the variation in the carbon number distribution for the deposits with the same total flow rate but different water cut is much less significant. For the total flow rate of 5 $m^3/h$ (shear stress at the wall at around 1−1.5 Pa), the carbon number distributions of the deposits become very close to that of the oil. As was discussed previously, a deposit completely formed by gelation has the same carbon number distribution of the oil above WAT, and it

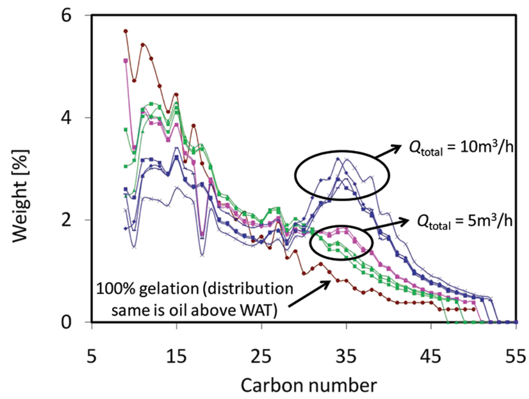


**Figure 12.** Carbon number distribution for the deposit with the experiments of different total flow rates.

is expected that the deposit formation in this group is highly gelation-driven. However, as the total flow rate increases to 10 $m^3/h$ (shear stress at the wall around 3.4−4.8 Pa), a significant amount of heavy components (C28+) is seen in the deposits, indicating that diffusion is the major mechanism in the formation of the deposits.

A close examination of the carbon number distributions of the deposits for the experiments with total flow rate of 5 $m^3/h$ reveals the variation as the water cut changes, which is shown in Figure 13.

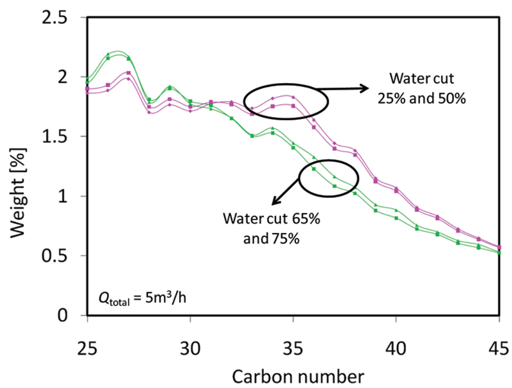


**Figure 13.** Carbon number distribution for the deposit with the experiments of different water cuts while the total flow rate is maintained at 5 $m^3/h$.

The deposits from the experiments with the water cut of 65% and 75% have smaller fractions of the heavy components. Their carbon number distributions are more similar to that of the oil when compared to the deposits from the experiments with water cuts of 25% and 50%, which indicates that gelation is more dominant in high water cuts. A possible explanation for this difference in the degree of gelation among the experiments with different water cuts can be found from the difference in the shear stress in the oil phase, which is known to defer gelation.[9,13] The distribution of the water volume fraction for the flows with these water cuts (Figure 10a) shows an increasing amount of water in the oil as the water cut increases from 50% to 80%. Therefore, this increasing degree of gelation is probably due to the increasing amount of water in the oil phase to reduce the viscosity of the mixture and thereby the shear stress (emulsion effects on the viscosity are not considered due to the presence of the emulsion breaker).

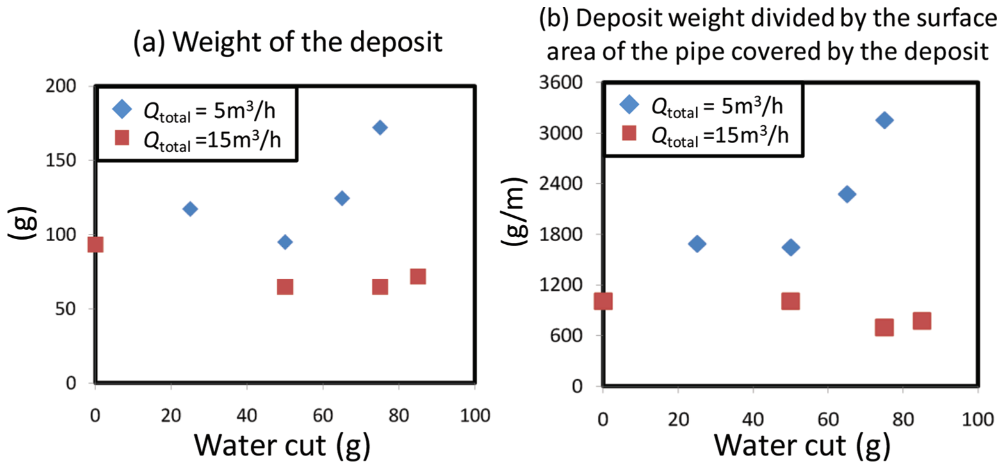


**Figure 14.** The weights of the deposit and the weights of the deposit per unit surface area of the pipe covered by the deposit.

*3.B.2. Deposit Weight versus Surface Area.* Figure 14a shows the weights of the wax deposit measured at the end of the experiments. It should be noted that the surface areas of the pipe covered by the wax deposit are different between experiments with different total flow rates and different water cuts, as shown in Figures 15 and 16. (The weight of the deposit for water cut of 10% and total flow rate of 10 $m^3/h$ is not listed because the duration of the experiment is different from the rest of the experiments of the same flow rate and different water cut.) Consequently, a more reasonable comparison would be the weights of the deposit divided by the arc areas covered by the deposit, which is shown in Figure 14b.

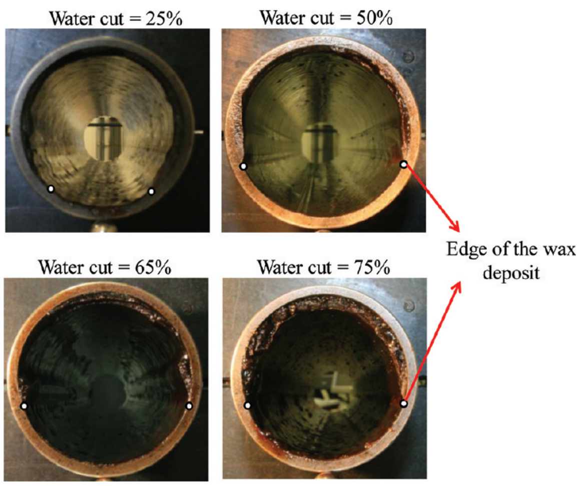


**Figure 15.** Camera pictures of the wax deposit for the experiments with total flow rate of 5 $m^3/h$.

It can be seen that the weights of the deposit for the deposition experiments with a total flow rate of 5 $m^3/h$ are higher than those with the total flow rate of 10 $m^3/h$. For the experiments with a total flow rate of 5 $m^3/h$, the thicknesses of deposits at the water cuts of 65% and 75% are higher than those at the water cuts of 25% and 50%. The degree of gelation and the thickness of the deposit for all of the experiments are listed in Table 6.

It can be seen that a decrease in the shear stress in the oil phase corresponds to an increase in the degree of gelation as well as the thickness of the deposit. This finding is consistent with the existing conclusions for single-phase flow that a decrease in the oil flow rate can lead to an increase in the thickness of the deposit and a decrease in the wax fraction of the deposit.[16]

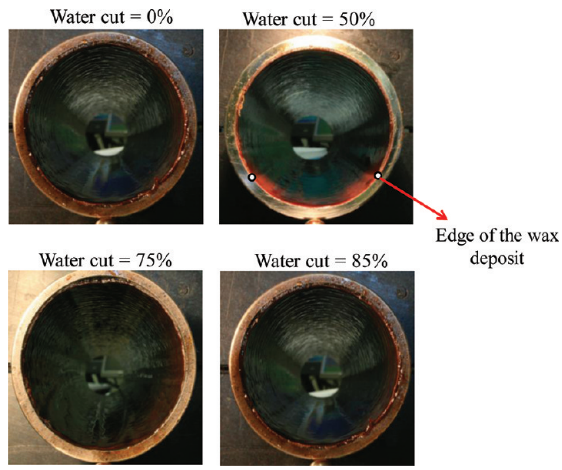


**Figure 16.** Camera pictures of the wax deposit for the experiments with total flow rate of 10 $m^3/h$.

**Table 6. Degree of Gelation and Thickness of the Deposit for the Experiments with Different Shear Stress**

| | $Q_{total}$ = 10 $m^3/h$ | $Q_{total}$ = 5 $m^3/h$ | |
|---|---|---|---|
| | | water cut 25–50% | water cut 65–75% |
| shear stress of the oil phase | highest | low | |
| degree of gelation | lowest | high | highest |
| deposit thickness | lowest | high | highest |

## 4. CONCLUSIONS

In this research, wax deposition experiments in oil/water two-phase stratified flow were carried out to investigate the effect of the presence of water on wax deposition. First, a flow map study was performed to identify the flow regimes for oil/water stratified flow. The X-ray measurement shows that completely stratified flow was achieved in the cases of water cut ranging from 30% to 60% at low total flow rate ($Q$ = 5 $m^3/h$). As the total flow rate further increases, the formation of the oil/water droplets reduces the degree of stratification, and even prevents stratified flow from occurring.

Wax deposition experiments were carried out at various water cuts with the total flow rates of 5 and 10 $m^3/h$. The GC analysis for the composition of the wax deposit further confirmed the coexistence of the two mechanisms in deposit formation: diffusion and gelation. For the experiments with a total flow rate of 5 $m^3/h$, it is seen from the GC analysis that deposits share similar compositions with the oil, indicating that the formation of the wax deposit is highly gelation-driven. The fractions of the heavy components in the deposits increase as the total flow rate increases from 5 to 10 $m^3/h$, indicating that the degree of wax gelation is reduced. This finding is consistent with the conclusion from the recent rheology studies, which show that increasing shear stress defers gelation. The weight measurements further revealed that the experiments with lower total flow rates (lower shear stress) yield a greater amount of wax deposit. This finding provides an alternative explanation for the existing wax deposition studies in single-phase flow that the deposit thickness greatly increased as the oil flow rate increased.[16]

As the degree of gelation is determined by a variety of elements including the shear stress, the cooling rate, the temperature, and the wax content of the oil, future work should be dedicated to extending the existing knowledge of these effects on gelation at quiescent conditions to flow conditions.

## ■ AUTHOR INFORMATION

### Corresponding Author

*E-mail: rahof@statoil.com.

### Notes

The authors declare no competing financial interest.

## ■ ACKNOWLEDGMENTS

We acknowledge financial support from the University of Michigan Industrial Affiliates Program from the following companies: Chevron, ConocoPhillips, Multiphase Solutions Kenny Inc., Nalco, Shell, Schlumberger, Statoil ASA, and Total.

## ■ REFERENCES

(1) Huang, Z.; Lee, H. S.; Senra, M.; Fogler, H. S. *AIChE J.* **2011**, *57*, 2955−2964.

(2) Akbarzadeh, K.; Zougari, M. *Energy Fuels* **2008**, *47*, 953−963.

(3) Burger, E. D.; Perkins, T. K.; Striegler, J. H. *J. Pet. Technol.* **1981**, *36*, 1075−1086.

(4) Labes-Carrier, C.; Rønningsen, H. P.; Kolnes, J.; Leporcher, E. *Wax Deposition in North Sea Gas Condensate and Oil Systems: Comparison between Operational Experience and Model Prediction*; 2002.

(5) Singh, P.; Venkatesan, R.; Fogler, H. S.; Nagarajan, N. *AIChE J.* **2000**, *46*, 1059−1074.

(6) Padgett, F. W.; Hefley, D. G.; Henriksen, A. *Ind. Eng. Chem.* **1926**, *18*, 832.

(7) Visintin, R. F. G.; Lapasin, R.; Vignati, E.; D'Antona, P.; Lockhart, T. P. *Langmuir* **2005**, *21*, 6240−6249.

(8) Abdallah, D. J.; Weiss, R. G. *Langmuir* **2000**, *16*, 352.

(9) Venkatesan, R.; Nagarajan, N. R.; Paso, K.; Yi, Y.-B.; Sastry, A. M.; Fogler, H. S. *Chem. Eng. Sci.* **2005**, *60*, 3587−3598.

(10) Rønningsen, H. P.; Bjorndal, B. *Energy Fuels* **1991**, *5*, 895−908.

(11) Senra, M.; Scholand, T.; Maxey, C.; Fogler, H. S. *Energy Fuels* **2009**, *23*, 5947−5957.

(12) Kane, M.; Djabourov, M.; Volle, J. L.; Lechaire, J.; Frebourg, P. G. *Fuels* **2003**, *82*, 127−135.

(13) Kane, M.; Djabourov, M.; Voile, J. L. *Fuel* **2004**, *83*, 1591.

(14) Wardhaugh, T. L.; Boger, V. D. *AIChE J.* **1991**, *37*, 871−885.

(15) Rønningsen, H. P. *J. Pet. Sci. Eng.* **1992**, *7*, 177−213.

(16) Hoffmann, R.; Amundsen, L. *Energy Fuels* **2010**, *24*, 1069−1080.

(17) Hoffmann, R.; Johnson, G. W. *Flow Meas. Instrum.* **2011**, *22*, 351−359.

(18) Valle, A. Three Phase Gas-Oil-Water Pipe Flow. Ph.D. Thesis, Imperial College of Science, Technology and Medicine, London, UK, 2000.